Perfluorocarbon nanodroplets stabilized by fluorinated surfactants: characterization and potentiality as theranostic agents

Astafyeva, K.; Somaglino, L.; Desgranges, S.; Berti, R.; Patinote, C.; Langevin, D.; Lazeyras, François; Salomir, Rares Vincent; Polidori, A.; Contino-Pépin, C.; Urbach, W.; Taulier, N.

How to cite

ASTAFYEVA, K. et al. Perfluorocarbon nanodroplets stabilized by fluorinated surfactants: characterization and potentiality as theranostic agents. In: Journal of Materials Chemistry B, 2015, vol. 3, n° 14, p. 2892–2907. doi: 10.1039/C4TB01578A

This publication URL: https://archive-ouverte.unige.ch/unige:98772

Publication DOI: 10.1039/C4TB01578A

Journal of Materials Chemistry B

PAPER

View Article Online
View Journal | View Issue

Cite this: J. Mater. Chem. B, 2015, 3, 2892

Perfluorocarbon nanodroplets stabilized by fluorinated surfactants: characterization and potentiality as theranostic agents

K. Astafyeva,[abc] L. Somaglino,[abc] S. Desgranges,[de] R. Berti,[abc] C. Patinote,[de] D. Langevin,[f] F. Lazeyras,[g] R. Salomir,[h] A. Polidori,[de] C. Contino-Pépin,[de] W. Urbach[ij] and N. Taulier*[abc]

We aim to produce emulsions that can act as contrast agents and drug carriers for cancer imaging and therapy. To increase tumor detection and decrease drug side effects, it is desirable to take advantage of the enhanced permeability and retention effect that allows nanoparticles to accumulate in tumor tissues. To do so, the emulsion droplets need to be small enough and stable over time in addition to enhancing image contrast and carrying a drug payload. In the present study, we have investigated the properties and potentiality as theranostic agents of perfluorocarbon emulsions stabilized by a biocompatible fluorinated surfactant called FTAC. To obtain better control of our system, the synthesis of those surfactants was studied and their physico-chemical properties were explored in different configurations such as micelles, in the perfluorocarbon droplet shell and at water/air and water/perfluorocarbon interfaces. The originality of this work lies in the determination of numerous characteristics of emulsions and fluorinated surfactants including surface tension, interfacial tension, critical micelle concentration, adiabatic compressibility, density, size distribution (aging studies), and ultrasonic echogenicity. These characterization studies were conducted using different types of FTAC and several perfluorocarbons (perfluoropentane, perfluorohexane, and perfluorooctyl bromide). We have also shown that a hydrophobic drug could be encapsulated in the FTAC-stabilized perfluorocarbon droplets thanks to triacetin addition. Finally, the perfluorocarbon emulsions were detectable *in vitro* by a clinical 3 T MRI scanner, equipped with a double frequency $^{19}F/^{1}H$ transmit–receive coil.

Received 22nd September 2014
Accepted 10th January 2015

DOI: 10.1039/c4tb01578a

www.rsc.org/MaterialsB

1 Introduction

Early detection of tumors and targeted drug delivery are two main objectives in treatments against cancer. A recent approach consists of using the well-known permeability of tumor vessels to large nanoparticles. Indeed, whereas normal vessels are permeable only to small molecules (<12 nm), tumor vessels present large inter-endothelial gaps (most tumors exhibit a gap cut-off between 400 and 800 nm) allowing the passage of nanoparticles.[1–4] Nanoparticles with a mean diameter of 100–300 nm have the best chance to use these gaps whatever the tumor type. In addition, tumors exhibit a dysfunctional lymphatic drainage system that induces the retention of nanoparticles in the tumor tissues.[1] These two properties represent the so-called enhanced permeability and retention (EPR) effect that allows passive tumor targeting by nanoparticles that act as drug carriers or/and contrast agents.[5,6] The best imaging modalities, associated with contrast agents and suited for tumor detection, appear to be contrast echography and magnetic resonance imaging (MRI). On the one hand, contrast echography has realtime imaging ability, offers a cheaper imaging alternative, and is available in most hospitals. On the other hand, MRI offers the best tissue contrast. Unfortunately, commercial contrast agents currently available for both techniques are not compatible with the EPR effect. Indeed, commercial ultrasound contrast agents are stabilized bubbles with a micrometer size (1–12 μm) that

[a]Sorbonne Universités, UPMC Univ Paris 06, UMR 7371, URM_S 1146, Laboratoire d'Imagerie Biomédicale, 75006 Paris, France. E-mail: nicolas.taulier@upmc.fr; Fax: +33 1 4633 5673; Tel: +33 1 4441 4969
[b]CNRS, UMR 7371, Laboratoire d'Imagerie Biomédicale, F-75006 Paris, France
[c]INSERM, URM_S 1146, Laboratoire d'Imagerie Biomédicale, F-75006 Paris, France
[d]Université Avignon, équipe Chimie Bioorganique et Systèmes Amphiphiles, IBMM UMR 5247, F-84000, Avignon, France
[e]Institut des Biomolécules Max Mousseron, UMR 5247, CNRS-Universités Montpellier I et II, F-34093 Montpellier, France
[f]Université Paris Sud 11, CNRS, UMR 8502, Laboratoire de Physique des Solides, Orsay, France
[g]Department of Radiology and Medical Informatics, University of Geneva, Switzerland
[h]Image Guided Interventions Laboratory, Faculty of Medicine, Radiology Department, University Hospitals of Geneva, Switzerland
[i]Université Paris Descartes, Paris, France
[j]Laboratoire de Physique Statistique de l'École Normale Supérieure, UMR CNRS 8550, 24 rue Lhomond, 75006 Paris, France

prevent them from extravasating out of the vasculature into the tumor tissue. Such bubbles also exhibit a rapid blood clearance, representing a strong barrier for their use as quantitative tracers or drug carriers. In contrast, commercial MRI contrast agents, commonly based on gadolinium, leak across even normal vessel walls. It may be possible to overcome the limitations of both imaging modalities by using perfluorocarbon (PFC) nanodroplets as contrast agents. Indeed, several studies have shown that perfluorocarbon droplets can be detected using ^{19}F MRI.[7–9] Unfortunately, the acoustic resonance frequency of such nanodroplets lies outside the clinical range of echography (1–15 MHz). However, they can still enhance ultrasound contrast when accumulated in a specific region or bound to a targeted surface.[10,11] But the best approach to significantly improve their echogenicity is the vaporization of the nanodroplets.[12–14]

Nevertheless, a major difficulty of the task lies in the production of stable droplets with a sufficient lifetime to allow an accumulation in tumor tissues using the EPR effect. Most perfluorocarbon droplets produced for imaging purposes were prepared as an emulsion and used lipids,[10,13,15,16] surfactants,[17,18] proteins,[19] or diblock polymers [20] as emulsifier. Although alkanes, a constituent part of emulsifiers, and fluoroalkanes are both hydrophobic molecules, they are not miscible.[21] Thus the above emulsifiers exhibit a very low affinity for perfluorocarbons. Droplets coated with these emulsifiers are not very stable. To overcome this problem, the best way is to replace the (lipophilic) hydrocarbon part of the emulsifier with a (lipophobic and fluorophilic) perfluorocarbon part. A convenient approach is to use fluorinated surfactants,[22] a few of them are commercially available, mostly from Dupont like Zonyl® (available up to 2010–2012), Capstone®, and Krytox®. These commercial surfactants were designed for industrial purposes but not for medical applications. Even if little is known about their toxicity, several studies have used them in contrast agent formulation.[19,23,24] Another fluorinated surfactant, called FTAC, was initially designed in the nineties as an oxygen carrier[25,26] and a drug carrier.[27,28] It was later used for the solubilization of membrane proteins.[29] FTAC exhibits good biocompatibility (no hemolytic activity, LD_{50} up to 4.5 g kg^{-1} in rats after i.v. administration) and ubiquitous distribution in rats after the i.v. or *per os.* route, and displays a long half-life (30–50 h) without any degradation in both plasma and tissues.[27]

Because of its biocompatibility, FTAC is an appealing candidate for producing perfluorocarbon-based colloids for theranostic purposes. However, the chemical and physical properties of FTAC still remain to be understood. For these reasons, we have characterized the properties of this fluorinated surfactant at interfaces, in solution as micelles, and as an emulsifier to stabilize droplets made of different perfluorocarbon liquids. Next, we have evaluated the overall characteristics of FTAC–perfluorocarbon nanoemulsions such as density, size distributions, aging, and ultrasound backscattering. Finally, we have assessed the theranostic capability of these emulsions as drug carriers and ^{19}F MRI contrast agents.

2 Materials and methods

2.1 Materials

Perfluoropentane (PFP), perfluorohexane (PFH), and perfluorooctyl bromide (PFOB) were purchased from ABCR GmbH & Co (Germany). The purity is 90, 95, and 99% for PFP, PFH, and PFOB, respectively. For tension measurements, PFOB was further purified through a column of activated neutral alumina (purchased from Sigma-Aldrich). Water was purified using a Purelab Option Q system from ELGA Labwater. Fluorinated surfactants were FTAC telomers (Fig. 1), the synthesis of which was described in previous papers.[30,31] We followed the published protocol as summarized below. Surfactants were obtained by free radical polymerization of an acrylamide monomer derived from Tris, the tris(hydroxymethyl) acrylamidomethane (THAM), or from its peracetylated analogue (tris(acetoxymethyl)acrylamidomethane) in the presence of a perfluoroalkanethiol as a transfer reagent called "telogen". The physico-chemical parameters of these telomers (molecular weight, hydrophilic lipophilic balance or HLB, critical micelle concentration or CMC) can be adjusted through both the starting material and the experimental conditions.[30,32] Telomerization experiments were respectively performed in methanol (MeOH), when the monomer THAM was used as the starting material, and in tetrahydrofuran (THF) for peracetylated THAM. The later monomer is required to obtain a Degree of Polymerization (DPn) higher than 15 according to Giusti *et al.*[33] due to the observed limited solubility of polyTris oligomers in methanol. Telomerization experiments (Fig. 2) were carried out by refluxing the monomer **1** or **2** in a dry and degassed appropriate solvent, under an argon atmosphere, in the presence of 1*H*,1*H*,2*H*,2*H*-perfluorooctanethiol or 1*H*,1*H*,2*H*,2*H*-perfluorodecanethiol as transfer reagents and AIBN (α,α-azobisisobutyronitrile) as a radical initiator. The AIBN concentration in the reaction mixture was ten times lower than the telogen one.[34] The reaction was monitored by thin layer chromatography and pursued until complete disappearance of each monomer (12 to 24 h).

For telomers prepared from monomer **2**, the solution was concentrated and subsequently precipitated in diethylether. The precipitate was dissolved in water and freeze-dried to give surfactants with DPn < 15 as white powders.

As regards peracetylated telomers, after the total disappearance of monomer **1**, a final treatment under Zemplén

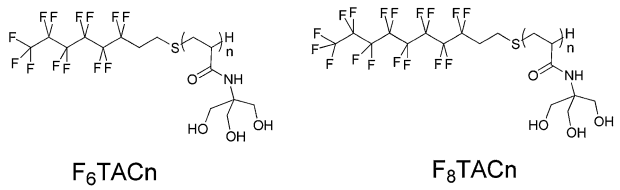

Fig. 1 The chemical structure of fluorinated surfactants F_iTAC_n is composed of a polar head made of *n* repeating Tris units (n = DPn is the degree of polymerization) and of a hydrophobic moiety made of fluorine atoms ($C_{i=6}F_{13}C_2H_4$ or $C_{i=8}F_{17}C_2H_4$).

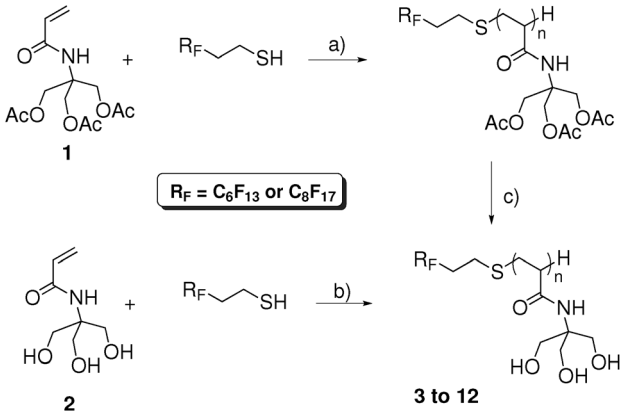

Fig. 2 Synthesis of fluorinated surfactants. Reagents and conditions: (a) AIBN/THF, reflux (62–66%); (b) AIBN/CH_3OH, reflux (62–73%); (c) MeONa cat./MeOH, room temperature (100%).

conditions yielded the telomers with DPn > 15 in satisfactory yields and NMR analysis confirmed the total disappearance of acetyl groups. These telomers were all purified by precipitation in MeOH/diethylether. The resulting precipitate was dissolved in water, then dialyzed overnight (cut off of 1000 Da). The solution was eventually freeze dried to obtain telomers as white powders.

Monoadduct (DPn = 1) derivatives of each telogen were also synthesized. These compounds were easily obtained from Michael addition reaction of the perfluoroalkylated thiol on monomer **2** according to the previously described conditions.[35]

2.2 Degree of polymerization determined by ^{19}F NMR

All spectra were recorded on a 250 MHz Bruker Avance I or II spectrometer with a resonance frequency of 235.3 MHz for ^{19}F. All data collection was performed without spinning the samples. ^{19}F-NMR spectra were acquired using the inverse-gated decoupling technique, each spectrum was the result of 256 scans with 131 072 data points using a relaxation delay of 4 s. Peak areas were integrated using manufacturer's standard software (1D WinNMR). A coaxial capillary was filled with a known solution of trifluoroacetic acid (TFA) sodium salt in D_2O (50 mg ml^{-1}) and put into a 5 mm diameter NMR tube in order to use as an external reference. 500 μl of solution was used in deuterated dimethyl sulfoxide (DMSO-d_6) for each sample (telomer or monoadduct) and the coaxial capillary was kept the same for all experiments. The TFA salt was chosen because of the proximity of the signal ascribed to its CF_3 group compared to that of the monoadduct's fluorinated tail (*i.e.* its telogen part), respectively at −75.96 and −80.15 ppm, thus avoiding the problem of keeping a uniform field over a long range. The ratio of the integration of the external standard (ICF_3 of TFA) over the integration of the monoadduct (ICF_3 of telogen) was plotted against the monoadduct molar concentration value to create a calibration curve. This molar concentration of monoadduct can be referred to as the molar concentration of its fluorinated telogen part. This calibration curve allows finding the molar concentration, M_{telogen}, of the telogen moiety of each telomer. All measurements were performed on triplicate samples, where each sample contained a precise mass of telomer dissolved in DMSO-d_6. The specific concentration of telomer, W_{telomer}, ranged from 3 to 12 g l^{-1}. Given that each telomer backbone contains a single telogen moiety, the average molecular mass of the telomer $\langle M_{\text{telomer}} \rangle$ can be calculated using:

$$\langle M_{\text{telomer}} \rangle = W_{\text{telomer}}/M_{\text{telogen}} \quad (1)$$

The average degree of polymerization (DPn) can thus be deducted through:

$$\text{DPn} = \frac{\langle M_{\text{telomer}} \rangle - M_{\text{F}}}{M_{\text{m}}} \quad (2)$$

where M_{F} and M_{m} are respectively the molecular mass of the perfluoroalkyl chain and of the monomer.

2.3 Emulsion preparation

About 10–50 mM of fluorinated surfactant FTAC was first solubilized in 2 ml of an aqueous solution made of deionized water and 2 mM of NaCl. The surfactant concentration was higher than its critical micellar concentration (CMC), as given in Table 1. A volume of 0.6 ml of perfluorocarbon liquid was added to the surfactant solution so that the molar ratio, N_{r}, of fluorinated surfactant molecules to perfluorocarbon molecules was known. Since the two liquids are immiscible, a two-phase solution was obtained, where the micelle aqueous solution was on the top and the perfluorocarbon liquid was at the bottom due to its higher density (see Table 2). The two-phase solution was prepared in a 15 ml centrifuge plastic tube that was placed in ice water. The tip end of an ultrasound cell disruptor (Branson Digital Sonifier, model 450) was put inside the solution at the interface between the micellar and perfluorocarbon liquids. Ultrasound was applied twice during 30 s using 0.5 s cycles at 20 kHz frequency with a waiting time of 10 min between the two insonification experiments. The newly prepared emulsion was eventually stored at 4 °C. Any volume of liquid perfluorocarbons that could not get encapsulated as a droplet would sediment after a few hours. If that was the case, only the top emulsion made of surfactant-stabilized perfluorocarbon droplets was retrieved and stored for further investigations.

2.4 Surface tension measurements

The surfactant surface activity at the air/water interface was determined by the Wilhelmy plate technique using a Krüss K100 tensiometer controlled by Labdesk software (Krüss, Germany). The platinum plate was cleaned by flaming before experiments. All solutions were prepared a night prior to measurements in purified water, the surface tension of which was $\gamma_{\text{S}} = 72.8$ mN m^{-1}. A 20 ml initial volume of a surfactant solution was placed in a glass trough and surface tensions were determined by diluting the solution. All measurements were carried out at 25 °C and repeated 3 times. The surface excess Γ_{S} at the air/water interface was calculated using the Gibbs

Table 1 Properties measured for several F_iTAC_n at room temperature. It includes the surfactant critical micelle concentration (CMC), the surfactant micelle diameter $D_{micelle}$, the surfactant partial adiabatic compressibility in a micelle $K^{\circ}_{S,micelle}$, the surface tension γ_S between air and water in the presence of the surfactant at the CMC, and the interfacial tension γ_I between water and PFOB in the presence of the surfactant. A comparison is given for surfactants: sodium laurate (NaL) and sodium dodecyl sulfate (SDS), and several lipids: 1,2-diacyl-*sn*-glycero-3-phosphocholines $(C_n)_2PC$, dipalmitoylphosphatidylcholine (DPPC), and decaglyceroldioleate (12-2-*O*)

Molecule	CMC (mM) ± 0.005	$D_{micelle}$ (nm) ± 0.5	$K^{\circ}_{S,micelle}$ (m^3 kg^{-1} Pa^{-1}) ± 0.2 × 10^{-13}	γ_S (mN m^{-1}) ± 0.4	γ_I (mN m^{-1}) ± 0.4
F_6TAC_7	0.36	7.9	1.4×10^{-13}	26	9.1
	0.35[a]				
	0.38[c]				
F_6TAC_{12}	0.614	8.3	0.7×10^{-13}	27.8	12.1
	0.32[a]				
F_6TAC_{13}	0.621	8.2	0.8×10^{-13}	31	12.1
F_8TAC_7	0.006	10.6	1.2×10^{-13}		10.7
	0.031[a]				11.8[a]
F_8TAC_{12}	0.020			31	
	0.035[a]				
F_8TAC_{13}	0.017	10.8	1.0×10^{-13}	31	10.4
NaL	7.1[b]				7.5[b]
SDS				18[e]	10[e]
					16[d]
$(C_6)_2PC$				31[d]	9.8[d]
$(C_7)_2PC$				28[d]	7.3[d]
$(C_8)_2PC$				25.5[d]	5.8[d]
$(C_9)_2PC$				24.8[d]	5.3[d]
$(C_{11})_2PC$				24[d]	4.4[d]
$(C_{12})_2PC$				24[d]	4[d]
DPPC					1[e]
12-2-O					6[e]

[a] Values extracted from Pavia *et al.*[18] [b] From Trevino *et al.*[48] [c] From Boyer *et al.*[49] [d] From Kabalnov *et al.*[50] [e] From Habif *et al.*[51]

adsorption isotherm equation $\Gamma_S = -\frac{1}{RT}\frac{d\gamma_S}{d \ln C}$, where γ_S is the surface tension (N m^{-1}) at the surfactant concentration C (mol l^{-1}).

2.5 Interfacial tension

The interfacial tension between water and perfluorocarbon liquid was measured with an error of 0.4 mN m^{-1} using a Tracker tensiometer (Teclis, France) at 25 °C. The tensiometer analyzes the shape of a reverse pendant water drop in perfluorocarbon liquid and fits it using the Young–Laplace equation to derive the interfacial tension. During the experiment, the water drop volume was kept constant at 6 mm^3 in the absence of a surfactant and at 2 mm^3 when the drop contained ~6 mM surfactant (above its CMC). We waited until the interfacial tension reached an equilibrium value to extract the interfacial

Table 2 The table displays molecular weight, M_w, boiling point, B_p, solubility in water S, diffusion coefficient in water, D, density ρ, sound velocity U, and adiabatic compressibility $K^{\circ}_{S,PFC}$ of three perfluorocarbon liquids. In addition there is adiabatic compressibility $K^{\circ}_{S,droplet}$ of a PFC droplet in water and the interfacial tension γ_I between PFC and water. Values without a footnote have been measured or calculated by us

	PFOB	PFH	PFP
Formula	$C_8F_{17}Br$	C_6F_{14}	C_5F_{12}
M_w (g mol^{-1})	498.99[a]	338.06[a]	88.05[a]
B_p (°C)	141–143[a]	57[a]	29[a]
S (mol m^{-3})	5×10^{-6}[b], 5.1×10^{-6}[c]	2.7×10^{-4}[d]	4×10^{-3}[d]
D (m^2 s^{-1})	5.2×10^{-10}	6.4×10^{-10}	7.0×10^{-10}
ρ (kg m^{-3})	1920, 1930[a], 1918[e]	1670, 1682[a]	1603, 1600[a]
U (m s^{-1})	631.8[f], 623.7[e]	548[g]	477[g]
$K^{\circ}_{S,PFC}$ (m kg^{-3} Pa^{-1})	6.9×10^{-13}	1.2×10^{-12}	1.7×10^{-12}
$K^{\circ}_{S,droplet}$ (m kg^{-3} Pa^{-1})	6.7×10^{-13}	1.3×10^{-12}	1.9×10^{-12}
γ_I (mN m^{-1})	48.7, 50.7[h], 51.8[i], 50[j]	38[k], 57.2[l], 55[c], 56.1[n]	56[m], 55[c]

[a] Are given by ABCR. [b] From Riess.[53] [c] From Kabalnov *et al.*[54] [d] From Kabalnov *et al.*[55] [e] Measured at 25 °C by Marsh *et al.*[56] [f] Measured at 21.3 °C by Hall *et al.*[57] [g] Measured at 25 °C by Cusco *et al.*[58] [h] From Pavia *et al.*[18] [i] From Kabalnov *et al.*[50] [j] From Habif *et al.*[51] [k] From LeGrand *et al.*[59] [l] From Nishikido *et al.*[60] [m] From Clasohm *et al.*[61] [n] From Halper *et al.*[62]

tension value, γ_I. As a test, we have also measured the interfacial tension of a sessile air bubble in water: a value of 72.5 ± 0.4 mN m^{-1} was measured.

2.6 Measurement of size by dynamic light scattering experiments

Mean hydrodynamic diameters and size distributions were measured at room temperature using an ALV-Correlator Goniometer System (ALV-CGS) from ALV Company. This device is equipped with a 22 mW He–Ne laser (λ = 632.8 nm) and a goniometer with an angular range from 17 to 152°. Samples were measured for angles varying from 60 to 120° at every 10° with a running time of 60 s for each angle. Measurements were performed in triplicate and the diameters were estimated with a precision of 0.5 nm. For emulsion samples, the droplet volume fraction, Φ, was in the range of (0.1–0.2) × 10^{-2} (*i.e.* 0.1–0.2%) to avoid multiple scattering effects. Micelle samples were prepared within a concentration range of 3–6 mM, higher than the surfactant CMC.

2.7 Size by Scanning Ion Occlusion Spectroscopy (SIOS)

The size distribution of droplets was measured using a Scanning Ion Occlusion Spectroscopy (qNano model from Izon Company, New Zealand).[36] The device principle is based on the Coulter effect.[37,38] For the measurement we used an elastomeric and resizable nanopore (NP) that covered a size range of either 70–200 nm (NP100), 100–400 nm (NP200), 200–800 nm (NP400), or 400–1600 nm (NP800). These ranges can be shifted by stretching the nanopore, in our case the applied stretching values were 45–48 mm. The voltage was set between 0.2 and 0.56 mV to keep the current baseline equal to approximately 120 nA. For each nanopore a calibration was made using calibrated plain polystyrene particles (purchased from Izon Company). Each sample was measured at two pressures: 3 and 5 cm of H_2O (1 cm ≈ 100 Pa), applied by a vapor pressure module. Samples were prepared in triplicate, and separately measured. For each sample a minimum of 500 counting events were collected and analyzed using Izon Control Suite 2.1 software. The analysis extracts the droplet size distribution, which in turn provides the droplet mean diameter and the polydispersity index, that is the ratio d_{90}/d_{10} where d_{90} and d_{10} are diameter values for which 90 and 10% of the distribution, respectively, has a diameter below these values. The closer to unity this index is, the more monodisperse the droplet size is. An error of less than 3% was obtained for the mean diameter and of 5–10% for the mode diameter.

2.8 Density and concentration

Density measurements were carried out at 25 °C using a digital density meter from Anton Paar (model DMA 5000 M). The device uses an oscillating U-tube sensor to derive densities with an accuracy of 5 × 10^{-6} g cm^{-3}. Density measurements were first used to estimate the specific concentration C (in mg ml^{-1}) of droplets in the emulsion. To do so, the droplet volume fraction, Φ, was derived from the mass conservation principle:

$$\Phi = \frac{\rho - \rho_o}{\rho_{droplet} - \rho_o} \quad (3)$$

where ρ is the density of the emulsion, ρ_o is the density of the solvent used for the emulsion, and $\rho_{droplet}$ is the density of a droplet. Measurements of the two first densities (*i.e.*, ρ and ρ_o) were straightforward, but the measurement of $\rho_{droplet}$ was not possible without knowing the droplet concentration. However, it could be derived using the equation:

$$\rho_{droplet} = \rho_{core}\Phi_{core} + \rho_{shell}(1 - \Phi_{core}) \quad (4)$$

where ρ_{core} and ρ_{shell} are respectively the densities of the perfluorocarbon core and of the fluorinated surfactant shell of a droplet. Φ_{core} and $(1 - \Phi_{core})$ are respectively the volume fractions of the perfluorocarbon core and of the surfactant shell. The value of ρ_{core} was taken as the density ρ_{PFC} measured for the corresponding bulk perfluorocarbon liquid (values are reported in Table 2), *i.e.* $\rho_{core} = \rho_{PFC}$. We assumed that the density of a fluorinated surfactant located in the droplet shell was close to the density of the same surfactant when it formed a micelle: $\rho_{shell} \approx \rho_{micelle}$. An average value of $\rho_{micelle} = 1440 \pm 30$ kg m^{-3} was measured for all surfactants. The shell volume fraction $(1 - \Phi_{core})$ could be calculated using an estimated value of the surfactant length and the value of the droplet mean radius. All estimations led to a value of $(1 - \Phi_{core})$ smaller than 0.12. We stated that taking $\rho_{droplet} = \rho_{PFC}$ instead of eqn (4) gave rise to a difference smaller than 3%. As this difference was reasonably small, we made the approximation $\rho_{droplet} \approx \rho_{PFC}$ in all calculations. Thus, the mass concentration, C, is given by:

$$C = \rho_{droplet}\Phi \approx \rho_{PFC}\frac{\rho - \rho_o}{\rho_{PFC} - \rho_o} \quad (5)$$

Finally, at a low concentration of droplets the partial volume V^o of a droplet was equal to the droplet apparent volume φ_V calculated using:[39]

$$\varphi_V = \frac{1}{\rho} - \frac{\rho - \rho_o}{\rho C}. \quad (6)$$

2.9 Ultrasound velocity measurements

Sound velocities of solutions were measured at 25 °C using a previously described differential resonator method,[40–43] at a frequency of 7.5 MHz. The solution filled a thermostated cell of a minimal volume of 0.8 ml where two lithium niobate piezotransducers faced each other. The analysis of the frequency–amplitude characteristic of the resonator was performed using an Agilent (model E5100A) network/spectrum analyzer. From this analysis we calculated variations in sound velocities with a precision of 0.15 cm s^{-1}. We eventually derived the specific sound velocity increment, $[u]$, due to the presence of a concentration C of droplets:

$$[u] = \frac{U - U_o}{U_o \times C} \quad (7)$$

where U and U_o are the sound velocities in the solution and in its solvent, respectively.

2.10 Adiabatic compressibility

Adiabatic compressibility β of a solution was obtained using Newton–Laplace's equation:

$$\beta = 1/(\rho U^2) \quad (8)$$

where U is the speed of sound in the solution that possesses a density ρ. The partial adiabatic compressibility of a solution was then calculated from:

$$K_S^o = \beta \times V^o \quad (9)$$

The apparent adiabatic compressibility φ_k of a droplet could be calculated using eqn (6)–(8):[44,45]

$$\varphi_k = \beta_o \times \left(2\varphi_V - 2[u] - \frac{1}{\rho_o}\right) \quad (10)$$

where β_o is the coefficient of adiabatic compressibility of the solvent. In our measurements, concentrations (in the 2–7 mM range) were low enough so that the apparent adiabatic compressibility of a droplet was equal to its partial adiabatic compressibility, *i.e.* $\varphi_k \approx K_S^o$.

2.11 Ultrasound backscattering measurements

The ultrasonic echogenicity of emulsions was determined from ultrasound backscattering measurements performed on a dedicated setup. Sample solutions were placed in a hollow cylindrical stainless steel chamber (30 mm in diameter and 3 mm in depth) maintained at 25 °C by a water circulation bath. The chamber was sealed with a cellophane membrane outstretched on a transparent tube. An ultrasonic focused transducer (model PI 50-2, Panametrics Inc., USA) was immersed in a water-filled tube. Its focal spot was positioned in the sample solution using a micro-control translation stage (VT-80, PI miCos, Eschbach, Germany). An optimized distance of 1.25 mm between the membrane and the center of the focal spot was used to minimize the influence of both sample solution attenuation and membrane vibrations on backscattered signals. The transducer was a 41 MHz PVDF transducer (34.25–47.75 MHz, −3 dB frequency bandwidth) with a 13 mm focal length and a 0.07×1 mm^2 (−3 dB) focal zone. Single short negative pulses (1 μJ energy) were generated in the sample at a 200 Hz repetition rate using a 200 MHz pulser–receiver (Panametrics Sofranel 5900 PR). Backscattered signals from the sample were received by the transducer/receiver set and digitized at a sampling rate of 2 GHz on a digital oscilloscope with a 8 bits vertical resolution (model WS424, Lecroy, USA). For each sample 100 signals were acquired and transferred to a personal computer for signal processing using MATLAB®. To select the zone of interest inside the sample, the signal processing consisted of the multiplication of each acquired signal by a Hann window of 2671 points (corresponding to the 1 mm length of the focal zone). The Power Spectrum density (PSD) of each resulting signal $s(t)$ was calculated. Both operations were made at once using the modified periodogram method of MATLAB. This method is almost equivalent of calculating PSD as follows: PSD $= |S(\nu)|^2$ where $S(\nu)$ is the Fast Fourier Transform of $s(t)$. The difference lies in the use of a normalization factor that compensates for energy losses due to windowing.

The echogenicity of an emulsion was finally evaluated in comparison to control measurements in water by calculating the Signal-to-Noise Ratio (SNR):

$$\mathrm{SNR}(f) = 10 \times \log\left(\frac{\mathrm{PSD_S}}{\mathrm{PSD_W}}\right) \quad (11)$$

where $\mathrm{PSD_S}$ and $\mathrm{PSD_W}$ are the mean Power Spectrum Densities over 100 PSD obtained in emulsion and in water, respectively. The calculation of an average PSD over many signals makes the SNR independent of particle configurations and, therefore, is representative of the so-called incoherent backscattered intensity.[46]

Finally, the mean value of SNR(f) over the transducer −3 dB frequency bandwidth, $\mathrm{SNR_{mean}}$, was extracted to characterize the echogenicity of an emulsion using a single quantity.

2.12 *In vitro* MRI

^{19}F MR spectroscopy and 3D imaging were performed on emulsions filling the bulb of a plastic Pasteur pipette. A transmitter–receiver, double frequency ^{19}F/^{1}H, saddle-type surface coil of 6 cm diameter (Clinical MR Solutions, Brookfield, WI, USA) was used with a 3 T MR scanner (Siemens Trio, Erlangen, Germany). Fourier Transform was applied to the FID signal acquired from the whole sample (BW 15 kHz corresponding to 125 ppm, sampling size of 4096 points, flip angle range 20 to 90°, NEX = 200, TR = 205 ms, TE = 0.35 ms). 3D imaging was performed with a nonselective pulse RF-spoiled GRE sequence, of main parameters: TR = 10 ms, TE = 3.25 ms, FA = 45°, voxel size $1.1 \times 1.1 \times 3$ or $3 \times 3 \times 3$ mm^3, NSA = 8, and acquisition time = 2 min 44 s.

2.13 Spectrofluorimetry

Fluorescence spectra were performed at 25 °C on samples filling a 1 cm quartz cuvette using a JASCO FP-6200 spectrofluorimeter. An excitation wavelength of $\lambda_{ex} = 363$ nm was used and spectra were recorded from 365 to 650 nm.

3 Results

3.1 Characterization of fluorinated surfactants

Taking into account published results about THAM telomerization,[18,30] we choose the values 5, 10, 15, 20, and 25 for the monomer over telogen ratio in order to obtain FTAC surfactants with a DPn (average number of repeating units on the polymeric backbone + 1 telogen moiety, Fig. 1) equal to 7, 13, 18, 22, and 27, respectively. The DPn value was assessed after FTAC surfactant synthesis by quantifying the fluorine on the hydrophobic tail using a ^{19}F-NMR methodology.[35,47] These measurements confirmed the expected DPn values with an error of ±1, in agreement with the literature. However, to further validate these results we also performed high-performance liquid chromatography (HPLC) measurements. HPLC data showed the presence of impurities along with FTAC surfactants. Their amount was small (<6%) for

DPn = 7–13, but significantly large (25–50%) for DPn > 13. After purification on a reverse-phase column, the impurities identified as poly-Tris (without a fluorinated tail) were completely removed. DPn measurements were performed again on purified samples. Surfactants that were previously tagged as having DPn values of 18, 22, and 27 were found after purification to possess a DPn no larger than 13 ± 0.5. The surfactants were noted F_iTAC_n where n is the degree of polymerization, DPn, and i reflects the number of carbons bearing fluorine atoms. The above syntheses were performed for surfactants having $C_6F_{13}C_2H_4$ or $C_8F_{17}C_2H_4$ as the hydrophobic moiety, *i.e.* $i = 6$ or 8. Eventually, we obtained the following surfactants: F_6TAC_1, F_6TAC_7, F_6TAC_{12}, F_6TAC_{13}, F_8TAC_1, F_8TAC_7, F_8TAC_{12}, and F_8TAC_{13}.

All these surfactants, except F_6TAC_1 and F_8TAC_1, could be solubilized in aqueous solutions up to a concentration of 100 mg ml^{-1}. A critical micellar concentration (CMC) had been determined for all solubilized surfactants (second column of Table 1). There is an order of magnitude of difference in CMC values between surfactants containing 6 and 8 carbons bearing fluorine atoms. The hydrodynamic diameters of FTAC micelles were measured using light scattering and above the CMC. Diameters of ~8 nm were measured for F_6TAC_n and ~11 nm for F_8TAC_n (third column of Table 1). The micelle density was derived from the micelle partial volume: $\rho_{micelle} = 1/\varphi_{V,micelle}$. Whatever the surfactant, we obtained $\rho_{micelle} = 1440 \pm 30$ kg m^{-3}. The measurements of the specific increment of sound velocity gave slightly different values depending on the surfactant. That is 35, 115, 105, 64, and 78 × 10^{-6} m^3 kg^{-1} for F_6TAC_7, F_6TAC_{12}, F_6TAC_{13}, F_8TAC_7, and F_8TAC_{13}. Using these values we have derived the partial adiabatic compressibilities of the micelles (Table 1, fourth column). In addition, we measured surface tensions at the water/air interface in the presence of surfactants at their CMC (Table 1, fifth column) as well as the interfacial tensions at the water/PFOB interface (Table 1, sixth column) in the presence of 7 mM surfactant. Finally, none of the FTAC surfactants could be solubilized in perfluorocarbon liquids.

3.2 Characterization of perfluorocarbons

Various properties of PFOB, PFH, and PFP are reported in Table 2. Among these properties we measured the densities of perfluorocarbon liquids as well as the partial adiabatic compressibilities of perfluorocarbon droplets stabilized by the various FTAC surfactants using eqn (9). The compressibility value of such droplets did not significantly depend on the surfactant structure as well on the droplet size. The average compressibility values are reported in Table 2 for each perfluorocarbon. For comparison, we calculated the partial adiabatic compressibility of a bulk perfluorocarbon liquid using eqn (8). For each perfluorocarbon, the compressibility of a droplet is close to the compressibility of the corresponding bulk perfluorocarbon. Finally, we calculated the diffusion coefficient, D, of a perfluorocarbon molecule in water at 25 °C as predicted by the Wilke–Chang equation:[52]

$$D = \frac{7.4 \times 10^{-8} (x M_w)^{0.5} T}{\eta v^{0.6}} \quad (12)$$

where η is the water viscosity, T is the temperature of water, M_w is the water molar mass, $x = 2.6$ is the association parameter of water, and $v = 1/\rho$ is the perfluorocarbon molar volume at the boiling point.

3.3 Optimization of the emulsion preparation

Emulsions were prepared in a 15 ml centrifuge tube using an ultrasonic homogenizer. We tested several tapered tips (with diameters of 3 mm, 5 mm, and 6.5 mm) and a 3 mm double stepped tip. Under our experimental conditions, only the use of a double stepped 3 mm tip gives rise to a homogeneous one-phase emulsion (as long as enough surfactant is added). Both the light scattering technique and scanning ion occlusion spectroscopy showed that such emulsions were made of droplets of mainly nanometer size (a typical example is shown in Fig. 3). In addition, emulsions with the smallest droplet average diameter and the narrowest size distribution of droplets were obtained when: the tip was positioned right at the interface between the aqueous and perfluorocarbon liquids, the ultrasonic power has reached 160 W (output power value given by the manufacturer), and the total sonication time was more than 60 s. Consequently, all samples were prepared using these optimal conditions.

3.4 Characterization of the stabilized droplets in emulsion

Emulsions were successfully produced with three perfluorocarbon liquids: perfluoropentane (PFP), perfluorohexane (PFH), and perfluorooctyl bromide (PFOB). After preparation the emulsions were stored at 4 °C to reduce the aging process. Then, we regularly monitored at room temperature the change in their size distribution and mean diameter using a scanning ion occlusion technique. Before any measurements, the emulsion was gently agitated. After a few minutes, a sample was taken from the upper part of the solution. In order to pinpoint which chemical and physical parameters affect droplet aging, we studied the size variation as a function of either the type of

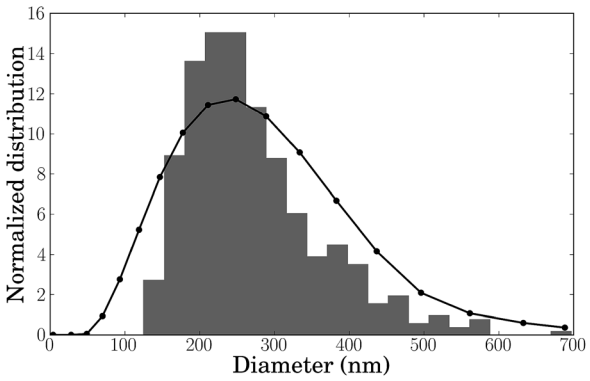

Fig. 3 Size distributions measured by SIOS (histogram) and DLS (solid line) of an emulsion made of F_6TAC_7 and PFOB in water.

liquid core, the type of surfactant, the ratio of surfactant to fluorocarbon, or the temperature.

An increase in the surfactant-to-fluorocarbon ratio N_r value from 0 up to 0.005 induced a dramatic decrease in droplet diameter whatever the perfluorocarbon used but did not alter the polydispersity. An example is given in Fig. 4 for PFOB droplets stabilized with the F_6TAC_7 surfactant, where the droplet mean diameter was reduced from 600 to 240 nm, while d_{90}/d_{10} remains equal to 2.3 ± 0.1. For larger ratios, no significant reduction in diameter was observed until a critical molar ratio, equal to 0.01 for PFOB and 0.006 for both PFH and PFP, where a stable foam was produced in addition to the emulsion droplets.

Next, to draw a comparison between emulsions, an identical surfactant-to-perfluorocarbon molar ratio N_r (=0.005) was used. Typical size distributions are displayed in Fig. 5 for droplets made of PFOB (black), PFH (gray), and PFP (light gray) stabilized with the F_6TAC_7 surfactant at day 0 (*i.e.* the day emulsions were prepared) and ninety days after the emulsion preparation. At day 0, a similar right skewed size distribution was observed for the three perfluorocarbons. As time passed, the size distribution widened, still keeping a right skewed shape. This broadening was always larger for PFP where a substantial number of droplets gained micrometer size. This process was slower for PFOB where most particles remained of nanometer size. Droplets' mean diameters were extracted from these size distributions and plotted as a function of time (see Fig. 6). The initial diameters ranged from 230 to 320 nm between the three perfluorocarbons. All the emulsions exhibited an increase in their droplet mean diameter and a broadening in their size distribution over time with a rate depending on perfluorocarbon. This rate was always the smallest for PFOB and the largest for PFP. Despite the increase in droplet size, all emulsions remained stable, at least up to 100 days. Indeed, all perfluorocarbon liquid was still in the form of a colloidal suspension as no phase transition was observed in the emulsions and no changes in sample density were detected.

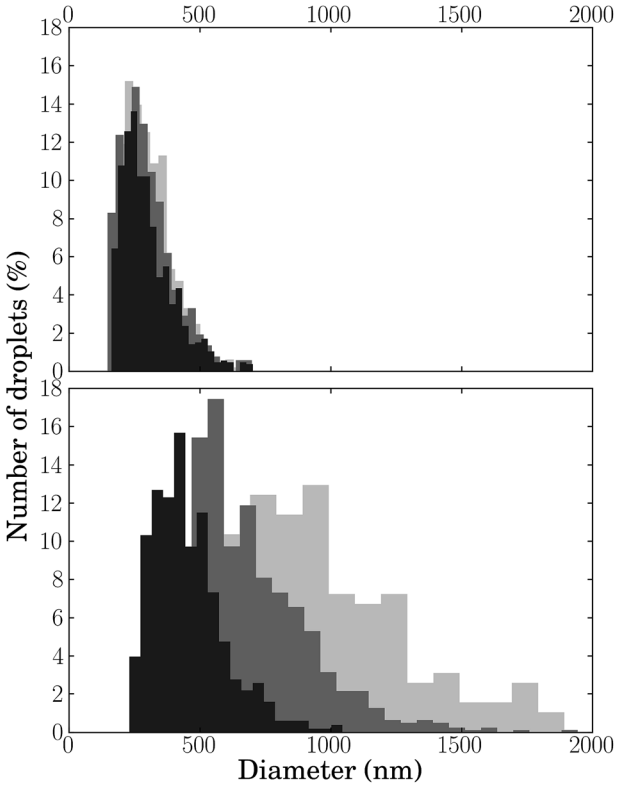

Fig. 5 Size distribution at day 0 (top) and day 90 (bottom) of droplets made of PFOB (black), PFH (gray), and PFP (light gray) and stabilized with the F_6TAC_{13} surfactant.

To study the effect of surfactant chemical structure on droplet size distribution, we used only PFOB emulsions as they exhibited the slowest change in size variation. Emulsions freshly prepared with F_6TAC_n and F_8TAC_n produced stable droplets with a similar mean diameter and size polydispersity

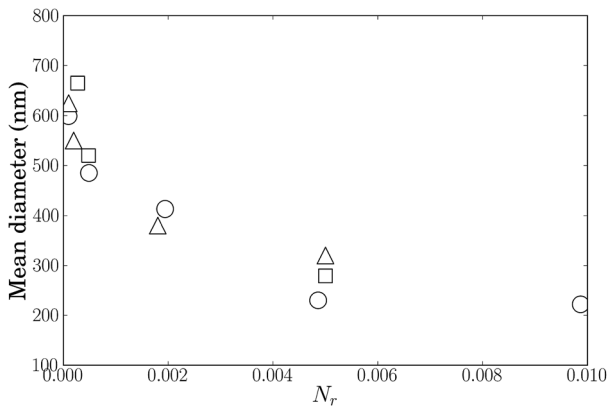

Fig. 4 Droplet mean diameter as a function of the surfactant to perfluorocarbon molar ratio N_r for F_6TAC_7–PFOB emulsion made of PFP (△), PFH (□), and PFOB (○).

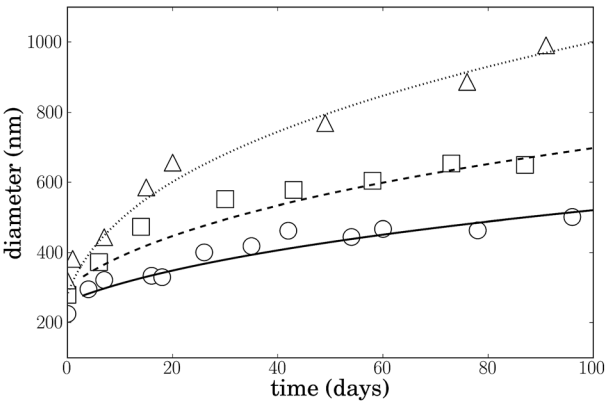

Fig. 6 Time variation of the droplet mean diameter when the droplet core was composed of perfluoropentane (△), perfluorohexane (□), and perfluoro-octyl bromide (○). For all emulsions, the volume fraction of droplets was $\Phi = 24 \times 10^{-2}$. The surfactant used was F_6TAC_{12} at an identical ratio $N_r = 0.005$. The lines represents the fit of the data using eqn (13): the derived Ostwald rates were $wf(\Phi) = 1.79 \pm 0.1$, 4.5 ± 0.3, and 14.1 ± 0.5 $nm^3\ s^{-1}$ for PFOB, PFH, and PFP respectively.

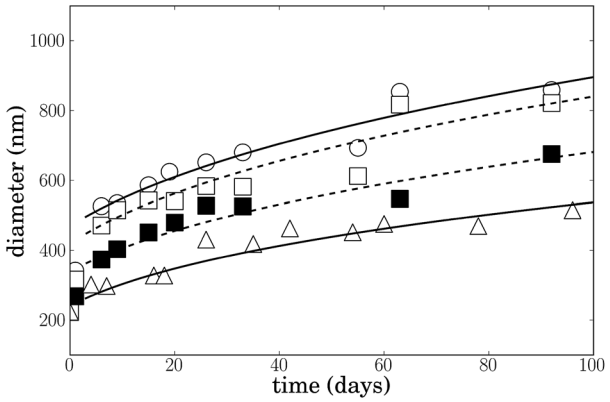

Fig. 7 Time-dependence of the droplet mean diameter of emulsions containing a volume fraction of PFOB droplets equal to $\Phi = 24 \times 10^{-2}$. For these emulsions $N_r = 0.005$ and the surfactants are F_8TAC_7 (○), F_6TAC_7 (□), and F_6TAC_{13} (△). The behavior of triacetin-loaded nanodroplets made of the F_6TAC_7 surfactant is also displayed (■). The lines represents the fit of the data using eqn (13) and gives Ostwald rate values: $wf(\Phi) = 8.9 \pm 0.7$ nm^3 s^{-1} for F_8TAC_7, 7.5 ± 0.7 nm^3 s^{-1} for F_6TAC_7, 4.0 ± 0.3 nm^3 s^{-1} for F_6TAC_7 in the presence of triacetin, and 2.0 ± 0.1 nm^3 s^{-1} for F_6TAC_{13}.

whatever the DPn value (see Fig. 7 at day 0). However, increasing the length of the surfactant hydrophilic head diminished the droplet size growth (see Fig. 7).

We also monitored the change in droplet size distribution when emulsions made of PFOB and F_6TAC_{13} were stored at several temperatures (4, 25, and 37 °C). As shown in Fig. 8, a small difference was observed between emulsions stored at 4 and 25 °C. However, the emulsions stored at 37 °C exhibited a faster growth in droplet mean size.

Finally, the aging process can be halted by freezing the freshly prepared emulsion, but the droplet coarsening is accelerated after thawing. Thus, the mean droplet diameter reaches 420 nm a day after thawing, whatever the time over which the emulsion was frozen.

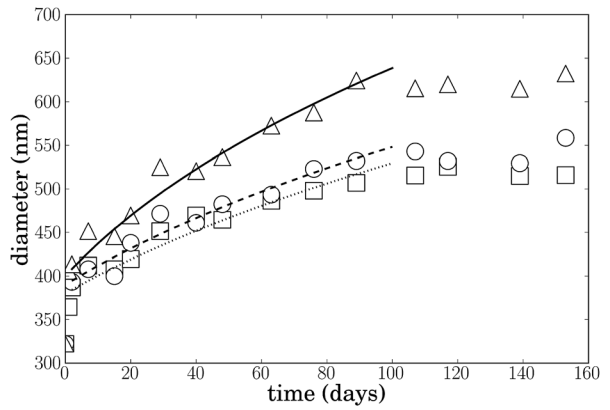

Fig. 8 Change in the mean diameter of PFOB droplets stabilized using F_6TAC_{13} ($\Phi = 24 \times 10^{-2}$), when the emulsions were stored at 4 (□), 25 (○), and 37 °C (△). The lines represents the fit of the data using eqn (13) and gives Ostwald rate values: $wf(\Phi) = 1.3 \pm 0.1$ nm^3 s^{-1} for 4 °C, 1.5 ± 0.1 nm^3 s^{-1} for 25 °C, 2.8 ± 0.1 nm^3 s^{-1} for 35 °C.

3.5 Encapsulation

Encapsulation studies were performed using a thalidomide derivative. Thalidomide is a drug world-wide known for tragic teratogenic effects reintroduced as a promising anticancer and anti-inflammatory agent.[63] Although the overall mechanisms by which thalidomide exerts its anti-tumor activity still remain to be elucidated, it is clearly demonstrated that it reduces the levels of proangiogenic factors such as VEGF, bFGF, HGF, as well as TNF-α and several interleukins, the latter being key drivers of inflammation. In this way, thalidomide appears as a "multi-target drug" with promising therapeutic potency in various disorders.[64] In 2010 we reported on the therapeutic potency of a 5-aminoalkylamino thalidomide analogue (called APA-thalidomide) in decreasing the clinical and pathological scores of experimental autoimmune encephalomyelitis (EAE).[65] A series of APA-thalidomides were prepared and evaluated on several biological targets for inhibition of angiogenesis and/or inflammation.[66] Among them, we recently developed a hydrophobic prodrug of APA-thalidomide, the *N*-benzyloxycarbonyl-glycine analogue of APA-thalidomide (called Z-Gly-Apathd), and used it as a model drug to investigate the capability of FTAC-stabilized perfluorocarbon nanodroplets for drug encapsulation. Actually, this derivative is a yellow fluorochrome the localization and release of which from droplets can be easily studied by spectrofluorimetry (Fig. 9 and 10).

The solubilization in liquid perfluorocarbons of Z-Gly-Apathd was not possible. However, we determined that up to 15 g l^{-1} of Z-Gly-Apathd could be solubilized in triacetin. Consequently, during the emulsion preparation, a part of the PFOB volume was replaced by a triacetin solution containing 5 g l^{-1} of the drug. Three triacetin-to-fluorocarbon molar ratios were investigated, that were 0.137, 0.272, and 1.37. For the last two ratios, a second phase with a yellow color was visible after emulsion preparation at the bottom of the sample. This suggested that the volume of triacetin containing the solubilized Z-Gly-Apathd could not be entirely encapsulated in the emulsion. Whereas the emulsion having a ratio of 0.137 was composed of only one phase homogeneously tinged with a yellow color, indicating that Z-Gly-Apathd was homogeneously distributed in the sample. For the latter ratio, 0.06 ml of PFOB was replaced by a triacetin/Z-Gly-Apathd solution during emulsion preparation, *i.e.* 10% of the droplet core volume was occupied by triacetin/Z-Gly-Apathd. By using the same molar ratio of triacetin-to-fluorocarbon (*i.e.* 0.137) we could also encapsulate Z-Gly-Apathd in emulsions made of PFH and PFP (data not shown).

After preparation, emulsions were carefully centrifuged (at 885 G, for a total time of 450 s), then washed (at every 90 s of

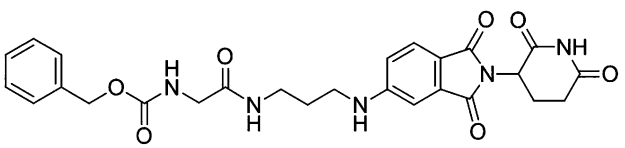

Fig. 9 Structure of the hydrophobic drug Z-Gly-Apathd that exhibits a high anti-angiogenic efficacy.

centrifugation) from the stock solution. The fluorescence spectra at $\lambda_{ex} = 363$ nm were measured for the washed triacetin-loaded emulsions in the absence and in the presence of Z-Gly-Apathd as well as for the filtered stock solution. No fluorescence signal was detected from the stock solution. The emulsion spectra were compared to the spectra obtained from triacetin solution (containing 5 mg ml^{-1} of Z-Gly-Apathd) and from pure PFOB liquid (see Fig. 10). The triacetin-loaded emulsion with no drug exhibited a single peak located at 412 nm as found for bulk PFOB. In the presence of Z-Gly-Apathd, the emulsion spectrum exhibited a second peak at 519 nm that was obviously characteristic of the drug signal. When the drug was solubilized in triacetin, a single peak was also observed but at 480 nm. Moreover, there was a negligible difference between the fluorescence spectra of the initial emulsion and the centrifuged and washed emulsion.

Additional emulsions were prepared by decreasing the ratio N_r in order to obtain suspensions mainly made of microdroplets where a fluorescent probe, fluorescein isothiocyanate (FITC), was solubilized in triacetin. Fluorescence microscopy showed that triacetin did not mix with PFOB but formed a corona between the PFOB core and the surfactant shell (data not shown).

Finally, the size growth rate was considerably reduced in the presence of triacetin. By following the time-dependence of the size of these triacetin-loaded PFOB droplets (see Fig. 7), we observed that they had grown from an initial mean diameter of 240 ± 10 nm to 430 ± 20 nm after 60 days (the addition of Z-Gly-Apathd did not modify these results). Whereas the mean diameter of triacetin-free droplets reached 700 ± 25 nm over the same period.

3.6 Ultrasound backscattering measurements

All backscattering measurements presented herein were performed on F_6TAC_{13}–PFOB emulsions. The impact of volume fraction on SNR_{mean} was evaluated on an emulsion prepared 7 days before experiments (mean diameter = 290 ± 10 nm, mode diameter = 200 ± 20 nm). For this purpose, dilutions were prepared from the initial emulsion solution to obtain several droplet volume fractions ranging from 0.1×10^{-2} to 2×10^{-2}. Each point in Fig. 11 represents a SNR_{mean} value obtained from a backscattering measurement performed on one sample. A good reproducibility in SNR_{mean} values was achieved for all volume fractions. Our data clearly show an increase in the SNR_{mean} value as the volume fraction increases, and this increase is steeper for diluted suspensions ($\Phi = 0.1$ to 0.5×10^{-2}) than for concentrated ones ($\Phi = 0.5$ to 2×10^{-2}). It should

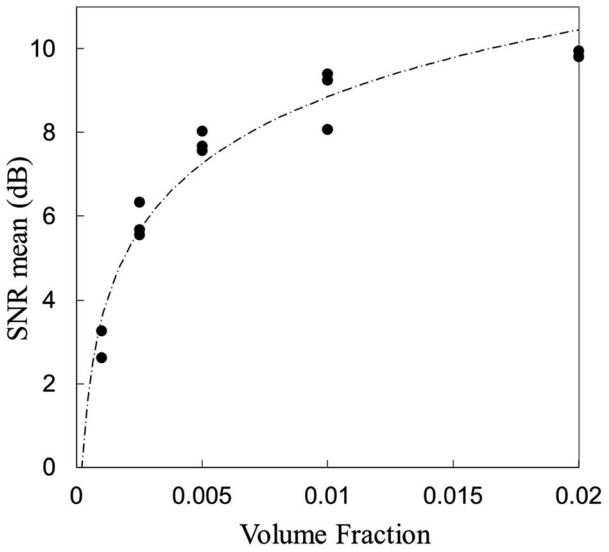

Fig. 11 SNR_{mean} as a function of droplet volume fraction extracted from backscattering measurements on F_6TAC_{13}–PFOB nanoemulsion (mean diameter: 290 ± 10 nm, mode diameter: 200 ± 20 nm).

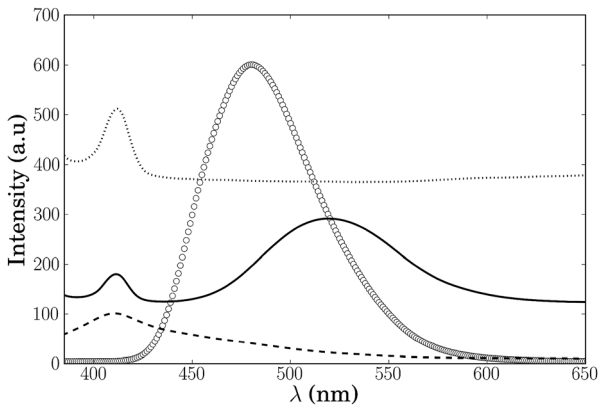

Fig. 10 Fluorescence spectra of Z-Gly-Apathd are displayed for Z-Gly-Apathd solubilized in bulk triacetin (circles) and when Z-Gly-Apathd is encapsulated in the F_6TAC_7–PFOB–triacetin droplets of an emulsion (continuous line). As controls, the spectra of bulk PFOB (dash line) and of the emulsion (F_6TAC_7–PFOB–triacetin) devoid of the drug (dotted line) are also displayed. All spectra were obtained at $\lambda_{ex} = 363$.

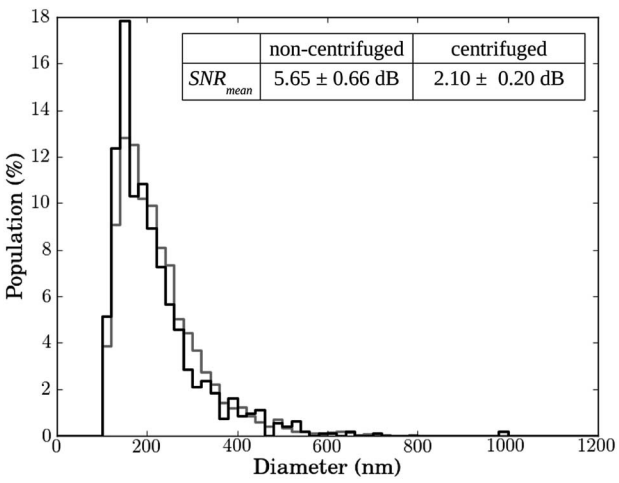

Fig. 12 Size distributions compared to backscattering measurements for a F_6TAC_{13}–PFOB nanoemulsion at $\Phi = 0.5 \times 10^{-2}$ before (black line) and after centrifugation at 885 g during 45 s (gray line). Mean and mode diameters were similar (within the error margin of the device): 235 ± 10 nm and 174 ± 20 nm, respectively, before centrifugation and 246 ± 10 nm and 175 ± 20 nm, respectively, after centrifugation.

be noted that the conditions of sonication did not alter the stability of emulsions, as we did not observe significant changes in both size distribution and density after backscattering measurements.

Secondly, the impact of larger droplets on the SNR_{mean} was evaluated by measuring ultrasound backscattering before and after gentle centrifugation (885 G, 45 s) of a fresh F_6TAC_{13}–PFOB emulsion (3 measurements for each solution). The droplet volume fraction Φ was kept at 0.5×10^{-2} for all backscattering measurements. Size distributions were monitored by SIOS before and after centrifugation as displayed in Fig. 12 along with SNR_{mean} values. We observed little differences in size distributions in the nanometer range as stated by the almost unchanged values of mean and mode diameters. However, a strong decrease in backscattered signals has been measured from the emulsion after centrifugation: the SNR_{mean} value was divided by 2.7. Looking more precisely at size distributions, we can see that even using a small nanopore (NP200), a few microdroplets could be detected before centrifugation but not anymore after centrifugation. Optical measurements using a microscope allowed detection of the presence of microdroplets before centrifugation but only a few of them remained after centrifugation.

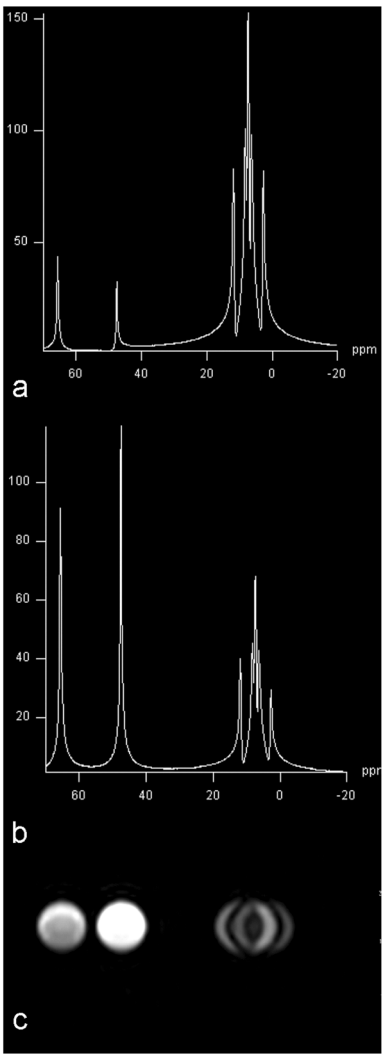

Fig. 13 Results of ^{19}F MRI measurements performed on an emulsion made of PFOB–F_6TAC_{13} droplets having a mean diameter of 400 nm and at a volume fraction of $\Phi = 5 \times 10^{-2}$. (a) and (b) Relative magnitude spectra, using a low (20°) and high (90°) flip angle respectively, TR = 205 ms. (c) Non-selective excitation heavily T1-weighted image of the same sample (TR = 10 ms, FA = 45°).

3.7 Potentiality of the emulsion as a ^{19}F MRI contrast agent

^{19}F MRI data were acquired on emulsions made of PFOB droplets stabilized with the F_6TAC_{13} surfactant, with a mean diameter of 400 nm and at droplet volume fractions ranging from 10^{-2} to 5×10^{-2}. All MRI spectra of emulsions exhibited five peaks (see Fig. 13) that are characteristic of pure PFOB since they were also observed in the spectra of pure PFOB. They possess different longitudinal relaxation rates and, within the current precision of measurement, these relaxation rates are not modified between emulsion and pure PFOB. In addition, measurements were performed on triacetin-loaded emulsions and triacetin/Z-Gly-Apathd-loaded emulsions of similar droplet sizes and at $\Phi = 5 \times 10^{-2}$. The absence of either triacetin or Z-Gly-Apathd in triacetin did not affect the peak location in the ^{19}F MRI spectra. Measurements were also carried out with pure micelles of F_6TAC_{13} in water.

4 Discussion

4.1 FTAC surfactant in aqueous solutions

By convention, the named F_iTAC_n used here signifies that there are i carbons bearing fluorine atoms. It differs from some other publications[18,67] where i represents the total number of carbon atoms in the surfactant hydrophobic tail, in this case i includes two additional carbons. Initially, we wished to produce FTAC surfactants with a polar head of increasing length, from n (or DPn) = 1 to 30, by following a published protocol on FTAC synthesis. We believed that the expected DPn values were achieved according to ^{19}F-NMR measurements. However, a HPLC analysis revealed that these results were biased due to the formation of the polyTris oligomer or polymer (without a fluorinated tail) as a side product in the synthesis of telomers with expected DPn over 12–13. The formation of this polyTris derivative can be ascribed to the faster consumption of the telogen compared to the monomer one, leading to a mixture made of low DPn (less than 13) fluorinated telomers and non-fluorinated oligomers or polymers. This side-reaction is probably due to the conditions of telomerization experiments applied for the synthesis of peracetylated telomers (see Fig. 2 conditions (a)) Indeed, the kinetic behavior of both monomer **1** (peracetylated THAM) and telogen reactants (perfluoroalkylthiol) seems to be strongly dependent on the nature of the solvent, as previously described by Loubat and Boutevin.[68] These authors reported an increase of the monomer consumption (resulting in high DPn values) when telomerization was performed in water rather than in organic media. In the future, mixtures of THF and water will be explored as reaction intermediates in order to reach a similar consumption of both monomer and telogen corresponding to

the ideal case of telomerization (*i.e.* transfer constant CT = 1). For now, we obtained FTAC with DPn = 1, 7, 12, and 13, but larger values could not be reached.

The water solubility of FTAC is directly correlated with their average degree of polymerization DPn. For FTACs having $C_6F_{13}C_2H_4$ and $C_8F_{17}C_2H_4$ fluorinated chains, it has been shown that their hydrosolubility occurs at DPn > 4.[69] Indeed, we could solubilize all of our FTAC surfactants in aqueous solutions, except for monoadduct ones (*i.e.* for DPn = 1). When solubilized in water, FTAC forms micelles above a critical micelle concentration (see Table 1) to shield their perfluorocarbon chain from water.[49] These micelles possess a diameter of ~8 and ~11 nm for F_6TAC_n and F_8TAC_n surfactants, that does not seem to depend on DPn values. Because fluoroalkanes are more hydrophobic than their hydrogenated counterparts, fluorosurfactants are less soluble in water and their CMC is much lower.[70] Pavia *et al.* did not observe a significant variation in CMC for DPn ranging from 4–5 to 12, whereas we observed a difference. Our CMC value almost doubled from DPn = 7 to 13. We also observed that the addition of a CF_2 group decreases the CMC by a factor of 30–60, while a decrease by a factor of 5–10 in the CMC is obtained by the addition of a CH_2 group to the hydrophobic tail of regular surfactants.[71]

4.2 FTAC surfactant at water/air and water/PFC interfaces

A characteristic feature of surfactants is to decrease the tension of an interface between an aqueous and hydrophobic environment like air or oil. Most of the data about surfactants concern the surface tension at the water/air interface. For comparison we performed such measurements and surface tensions of about 26–31 mN m^{-1} were obtained for FTAC surfactants. These values are close to what can be measured for non-fluorinated surfactants, that is in the range of 24–54 mN m^{-1}.[71]

The measurement of the interfacial tension between water and perfluorocarbon liquid is more relevant for perfluorocarbon emulsions since this parameter will dictate the stability of the droplet as well as its temperature of vaporization. Unfortunately, data are scarce in this domain. Most published measurements were performed at the PFOB/water interface, their values are reported in Table 1. In the absence of surfactants, our value of interfacial tension at the water/PFOB interface is about $\gamma_I = 48.7$ mN m^{-1}, close to the values (51 ± 1 mN m^{-1}) reported in the literature. The addition of FTAC logically decreased the interfacial tension. While there is no difference in γ_I values between F_6TAC_7 and F_8TAC_{13}, we measured a significant difference between F_6TAC_7 and F_6TAC_{12} or F_6TAC_{13}. Surprisingly, the order of magnitude of these values is similar to what has been measured for non-fluorinated surfactants (7–16 mN m^{-1} for NaL and SDS) and even larger than for lipids (1–10 mN m^{-1} for $(C_n)_2PC$, 12-2-*O*, and DPPC) (see Table 1). Bertilla *et al.*[72] showed that the interfacial tension in the presence of lipids can be further decreased by adding semi-fluorinated surfactants to the perfluorocarbon liquid: from ~24 mN m^{-1} for DMPC, DLPC, and PLC8 down to ~2 mN m^{-1}.

4.3 FTAC as emulsifier for perfluorocarbon/water emulsions

Various approaches exist for emulsion preparation, among them are stirring,[73] high-pressure microfluidizing,[74] ultrasonic homogenizing,[73,75] and microfluidics.[76] Ultrasonic homogenizing was chosen because it is a technique that is more easily found in laboratories. On the downside, it has been shown that the characteristics of an emulsion prepared by sonication depend on various parameters.[75] These parameters include the type of vessel containing the emulsion, the quantities of added solvent, the type of ultrasonic tip, the power applied on this tip, the time of sonication, and the position of the tip in the sample. We have optimized our ultrasonic parameters by using a plastic centrifuge tube of 15 ml and keeping the volumes of perfluorocarbon and aqueous solutions always the same, *i.e.* 0.6 and 2 ml respectively.

Our DLS and SIOS measurements showed that the prepared samples were a suspension of perfluorocarbon droplets as confirmed by our compressibility measurements. Indeed, the value of the droplet partial compressibility was similar to the value of bulk perfluorocarbon liquid. In addition, it was possible to predict the emulsion density with a good accuracy based on the added volumes of bulk perfluorocarbon and aqueous liquids, the densities of which were separately measured. Thus, the surfactant contribution to density and compressibility appears to be negligible. At the day of preparation (*i.e.* day 0), the droplet exhibited a size that was mainly in the nanometer range but with a significant polydispersity ($d_{90}/d_{10} = 2.3 \pm 0.1$). If the initial mean diameter was 230 nm for PFOB, 280 nm for PFH, and 320 nm for PFP (Fig. 6), particles up to 700 nm (Fig. 5) were easily detected on SIOS using a stretchable nanopore NP200 the initial (*i.e.* barely stretched) covered size range of which is 100–400 nm. Larger microscopic droplets were also visible under a microscope. Additional SIOS investigations using larger nanopores allowed us to estimate that these large particles (>700 nm) represent less than 1% of the total droplet volume fraction. It was possible to remove these microparticles using centrifugation, while filtering led to a destabilization of the emulsion.

In the absence of a surfactant, droplets are expected to coalesce, exhibiting an exponential increase in mean diameter according to the van den Tempel theory.[77,78] The presence of FTAC surfactants should prevent coalescence through steric interactions if the whole droplet surface is coated by a surfactant.[79] However, after sonication, the newly formed droplets are not immediately fully coated by surfactants, leaving some time for droplet coalescence. Once all the surfactant present is located on the droplet surface, coalescence may still continue to take place until the droplet surface has reduced enough (*i.e.* increase in the volume and decrease in the number) to obtain a full coating. This process explains why adding less surfactant leads to larger droplets as shown in Fig. 4. Whereas, if more surfactant is added than that could be borne by all droplet surfaces, the surfactant will form micelles. At high concentration ($N_r > 0.006$), this additional surfactant will lead to stabilization of the bubbles created by the sonication process and be responsible for the foam formation observed in our samples.

However, even if the coalescence is suppressed by surfactants, an increase in droplet mean diameter will still be observed over time. This behavior can be ascribed to the Ostwald ripening (OR) or molecular diffusion, that has been shown to occur for perfluorocarbon emulsions stabilized with phospholipids[50] and fluorinated surfactants.[53] This process is described by the Lifshitz–Slyozov–Wagner (LSW) model,[80–82] which predicts a linear relationship between the cubic mean radius R^3 and time t:

$$\frac{dR^3}{dt} = \frac{8}{9}\frac{S\gamma_I V_m{}^2 D}{RT} f(\Phi) = wf(\Phi) \quad (13)$$

where in our case, γ_I is the interfacial tension at the water/perfluorocarbon interface (in the presence of a surfactant), S and D are respectively the solubility and the diffusion coefficient of perfluorocarbon in water, V_m is the perfluorocarbon volume, R is the gas constant, T is the absolute temperature, $f(\Phi)$ is a correction factor taking into account the droplet volume fraction (=1 at low dilution), and w is the rate of the molecular diffusion of a perfluorocarbon molecule. We used eqn (13) to fit all our aging curves involving mean diameters and values of $wf(\Phi)$ are reported in the figure legends. In these fits, we systematically discarded the first points (*i.e.* at day 0 and day 1) to obtain an acceptable fit for PFOB and PFH, but we did not observe this problem for PFP. The problem is also reduced by increasing the temperature, indeed for emulsions kept at 37 °C only the measurements made at day 0 were discarded. This reflects the fact that Ostwald ripening started to be dominant after a few days. From our fits, we observe that the "corrected" Ostwald rate $wf(\Phi)$ increases when DPn decreases (Fig. 7) or temperature (Fig. 8) increases. These results are understandable as surfactants with longer polar heads provide a better barrier against the passage of perfluorocarbons and higher temperature increases the perfluorocarbon solubility in water. $wf(\Phi)$ naturally depends on the perfluorocarbon liquid used in droplets (see Fig. 6) since PFC possesses different properties.

It was possible to directly derive w since all parameters in eqn (13) have been determined. Several models provide an estimation of the value of $f(\Phi)$.[83] For a volume fraction of $\Phi = 24 \times 10^{-2}$, $f(\Phi)$ is equal to $\approx 2.2 \pm 0.3$ in most models. However, it should be emphasized that during emulsion storage droplets sediment. This may locally induce a higher fraction volume, hence the value of $f(\Phi)$ can be much larger. When taking $wf(\Phi) \approx 2.2$, we obtain $wf(\Phi) = 1.7$ nm^3 s^{-1} for F_6TAC_{12} and F_6TAC_{13}, in good agreement with the values derived from the fits in Fig. 6–8. For PFOB, the calculation of $wf(\Phi)$ slightly varies, from 1.2 to 1.7 nm^3 s^{-1}, depending on FTAC. Whereas fits of Fig. 7 show a variation from 2 to 9 nm^3 s^{-1}. As the properties of PFOB should be the same between the various FTAC and the error measured in γ_I is small, this disagreement probably comes from differences in the values of $f(\Phi)$. Indeed, a larger droplet size induces a faster sedimentation and hence a larger local volume fraction. Besides, still keeping $f(\Phi) \approx 2.2$, we obtain for F_6TAC_{12} the values $wf(\Phi) = 67$ nm^3 s^{-1} and $wf(\Phi) = 862$ nm^3 s^{-1} for PFH and PFP, respectively. These values are too different from the values derived from Fig. 6 only due to a variation in $f(\Phi)$ values. This disagreement is probably due to a wrong estimation of the perfluorocarbon solubilities in water. These values were, indeed, derived by Kabalnov *et al.* using eqn (13) to fit experimental data recorded for several hours (up to a few days).[54,55] In their case the extracted Ostwald rate is much higher than our rate measured over several months.

Taking Fig. 8, we observed that the Ostwald ripening process takes place for 100 days, as a fit by eqn (13) was only possible during this period. After this period the droplet mean diameter remained constant for a longer time but there is no satisfactory explanation for this behavior.

Finally, for an emulsion made of F_6TAC_{13} and PFOB, the replacement of the solvent by a saline 9‰ NaCl solution (for intravenous injection purposes) did not change the aging behavior for at least 30 days.

Our data show that despite the fact that our emulsions are not thermodynamically stable systems, they exhibit a lifetime of a few months. Indeed, after droplet sedimentation, a homogeneous sample is easily recovered after gentle stirring. Consequently, the emulsions can be either simply stored in a fridge or put in a freezer for a longer storage time, depending on the maximum droplet mean size we wish not to exceed.

4.4 Ultrasound backscattering measurements

The two-step increase behavior of SNR_{mean} observed with droplet volume fraction is well known. Many experimental and simulation studies, including those dealing with perfluorocarbon particles,[8,84] have reported such a result. In all these studies, the incoherent backscattered signal intensity also increases dramatically with volume fraction for dilute suspensions. Indeed, theoretical models (Morse and Ingard,[85] Faran[86]…) predict that for diluted small spherical particle solutions, the incoherent scattered intensity by N particles is the sum of the scattered intensity by each particle. Those models are valid only if: (1) the incident wavelength $\lambda > 2\pi R$ (R is the particle radius), (2) the region F containing the scatterers is considerably larger than λ, and (3) the region F is far from the transducer. As all those criteria are met in the present study, it can be assumed that the first part of the curve is representative of such behavior, also often referred to as Rayleigh linear scattering. In the present study, SNR_{mean} does also include attenuation mechanisms that prevent the curve from being fully linear.[87] Those mechanisms can be taken in account by applying some appropriate correction factors to the measured signals. In that case, only the incoherent backscattered waves are represented and a linear curve can be obtained.[23] For concentrated suspensions, the SNR_{mean} reaches a plateau which is representative of multiple scattering as well as attenuation effects. Briefly, in concentrated suspensions, backscattering from region F cannot be considered anymore as a simple sum of the contribution of every particles as the short distance between particles leads to strong interactions (re-scattering and absorption of scattered waves).[85]

Thus, the concentration has a significant impact on backscattering intensity, but the droplet size has even a higher impact on it. Indeed, Morse and Ingard predicted that the scattering cross-section for a particle is directly proportional to

the sixth power of its radius as well as to the fourth power of its incident wave frequency (see *Born approximation* eqn (8.2.19) (ref. 85)). Then, in a given frequency range, it is critical to check for the presence of microparticles in the emulsion, even if their concentration is very low. Our centrifugation experiment clearly illustrates that point with a SNR_{mean} divided by almost 3 after centrifugation which means that the Power Spectral Density was reduced by nearly a cube root. A more detailed quantification of these microparticles with a SIOS technique as well as their precise impact on the backscattered signal will be investigated in a future study.

In summary, the present study shows that backscattering measurement is a very sensitive tool for the detection of small amounts of liquid PFC microparticles in heterogeneous micro/nano-particle suspensions. Those microparticles can totally change the ultrasonic properties of solutions and are usually formed in emulsions. Thus, a special care should be given to remove those microparticles. Finally our results show that the weak echogenicity of liquid perfluorocarbon nanoparticles prevents their use as ultrasound contrast agents in agreement with the investigation of Couture *et al.*[23]

4.5 Potentiality of the FTAC stabilized nanodroplets as theranostic agents

Both hydrophilic and hydrophobic drugs cannot be solubilized in liquid perfluorocarbons. Consequently, to help drug solubilization in perfluorocarbon droplets, an additive solvent is required. In our case, we were interested in the encapsulation of a fluorescent thalidomide derivative (Z-Gly-Apathd). This hydrophobic prodrug has recently exhibited an interesting and unexpected anti-apoptotic effect in a photodynamic therapy (PDT) induced apoptosis model (unpublished result). Since liposoluble drugs, like thalidomide derivatives or paclitaxel, can be solubilized in oil, the more convenient way would be to use oil as a drug solvent. In the past, vegetable oils such as soya bean oil, olive oil, and canola oil have been mostly used in perfluorocarbon drug carriers.[7,88,89] Unfortunately, Z-Gly-Apathd exhibited a poor solubility in these oils (less than 0.1 g l^{-1}). Instead, we used triacetin, a simple and biocompatible triglyceride, which could dissolve up to 15 g l^{-1} of Z-Gly-Apathd. Our fluorescence results show, indeed, that the addition of a volume of solubilized drug in triacetin during emulsion preparation led to the drug encapsulation. However, the triacetin solution did not get solubilized in perfluorocarbon, instead it formed a corona between the perfluorocarbon droplet and the surfactant shell. Since 5 g l^{-1} of triacetin was occupying 10% of droplet volume, a total of 3 mg of drug was encapsulated in the 2.6 ml of emulsion. Interestingly, the presence of triacetin reduced the growth rates of the droplet size (as well as its polydispersity from $d_{90}/d_{10} = 2.3$ to 1.9 ± 0.1). A similar result was described for perfluorocarbon emulsions prepared by the addition of hexadecane in the droplets.[90]

In addition, our preliminary data show that PFOB nanoemulsions could be detected *in vitro* at a volume fraction of 1×10^{-2} by ^{19}F MR spectroscopy and imaging at 3 T, with isotropic $3 \times 3 \times 3$ mm^3 voxel size. In our measurements, a 3D matrix sized $128 \times 64 \times 40$ was acquired in 6 m with an average SNR value of 3.35 for the highest signal peak, determined after reduction of bias in GRE magnitude data according to Gudbjartsson and Patz.[91] Note that the ^{19}F detection coil used in this study can be further optimized, for instance, by upgrading to a bird-cage quadrature type which should improve both the sensitivity and spatial homogeneity of the signal. The detected ^{19}F MRI signal of the FTAC–PFOB nanoemulsion has mainly the characteristics of pure PFOB, even with the addition of triacetin. It is interesting to note that samples made of only fluorinated surfactant micelles in water can be detected and present a specific spectrum. However, in the spectra of FTAC–PFOB nanoemulsion samples, the characteristic peak of the FTAC surfactant is buried in the noise.

The benefit of having stable nano-agents with both imaging and therapeutic ability would be an asset in the evaluation of cancer treatment. Indeed, currently commercialized nanodrug carriers such as liposomes (for example Doxil®/Caelyx®) cannot be imaged. Consequently, it is not possible to assess if these carriers have extravasated into tumor tissues (*i.e.* especially for tumors with neovascularization that is not developed enough or that exhibits too small inter-endothelial gaps). The treatment fails if the carrier accumulation in such tissues is not sufficient, and precious time that could have been used for an alternate treatment is lost.

5 Conclusion

It was possible to prepare emulsions with PFOB, PFH, and PFP, where FTAC surfactants form the droplet shell and help to prevent droplet coalescence. The droplet mean diameter of an emulsion could be as small as 230 nm for PFOB but constantly increased for the first 100 days due to Ostwald ripening. All size distributions were right skewed with a small amount of microdroplets (<1%) that can be removed by centrifugation. In addition, these microdroplets appeared to be the main contributor to the signal backscattered by emulsions in our ultrasonic measurements. In their absence, the signal-to-noise ratio is small that prevents any use of a suspension of nanodroplets as ultrasound contrast agents, unless they could be vaporized. However, the suspensions of nanodroplets could be detected *in vitro* in a clinical 3 T MRI scanner, which opens the door for their further *in vivo* investigations as ^{19}F MRI contrast agents. Furthermore, we succeeded in encapsulating a hydrophobic drug in the perfluorocarbon droplets by adding triacetin, which is a first step toward the study of the localized therapeutic ability of such agents. In the next step we will study the toxicity and therapeutic effect of our emulsions on tumor cells *in vitro* and assess their potential as theranostic agents in small animals.

Acknowledgements

This work was supported by the grant ANR-10-NANO-06 overseen by the French National Research Agency (ANR) as part of the "Investissements d'Avenir", a grant "Émergence UPMC 2010" (project NACUNAT) from the University Pierre et Marie

Curie, and the Swiss National Foundation of Science grant number 31NM30_152045. The authors thank Dr Jean-Noël Hyacinthe (from the Biomedical Image Center (CIBM), University of Geneva) for providing the 3D ^{19}F MRI sequence.

References

1 Y. Matsumura and H. Maeda, *Cancer Res.*, 1986, **46**, 6387–6392.
2 F. Yuan, M. Dellian, D. Fukumura, M. Leunig, D. A. Berk, V. P. Torchilin and R. K. Jain, *Cancer Res.*, 1995, **55**, 3752–3756.
3 S. K. Hobbs, W. L. Monsky, F. Yuan, W. G. Roberts, L. Griffith, V. P. Torchilin and R. K. Jain, *Proc. Natl. Acad. Sci. U. S. A.*, 1998, **95**, 4607–4612.
4 H. Hashizume, P. Baluk, S. Morikawa, J. W. McLean, G. Thurston, S. Roberge, R. K. Jain and D. M. McDonald, *Am. J. Pathol.*, 2000, **156**, 1363–1380.
5 H. Maeda, H. Nakamura and J. Fang, *Adv. Drug Delivery Rev.*, 2013, **65**, 71–79.
6 Y. H. Bae and K. Park, *J. Controlled Release*, 2011, **153**, 198–205.
7 G. M. Lanza, X. Yu, P. M. Winter, D. R. Abendschein, K. K. Karukstis, M. J. Scott, L. K. Chinen, R. W. Fuhrhop, D. E. Scherrer and S. A. Wickline, *Circulation*, 2002, **106**, 2842–2847.
8 E. Pisani, N. Tsapis, B. Galaz, M. Santin, R. Berti, N. Taulier, E. Kurtisovski, O. Lucidarme, M. Ourevitch, B. T. Doan, J. C. Beloeil, B. Gillet, W. Urbach, S. L. Bridal and E. Fattal, *Adv. Funct. Mater.*, 2008, **18**, 2963–2971.
9 R. Díaz-López, N. Tsapis and E. Fattal, *Pharm. Res.*, 2010, **27**, 1–16.
10 M. S. Hughes, J. N. Marsh, C. S. Hall, R. W. Fuhrhop, E. K. Lacy and G. M. Lanza, *J. Acoust. Soc. Am.*, 2005, **117**, 964–972.
11 J. N. Marsh, K. C. Partlow, D. R. Abendschein, M. J. Scott, G. M. Lanza and S. Wickline, *Ultrasound Biol. Med.*, 2007, **33**, 950–958.
12 N. Y. Rapoport, A. M. Kennedy, J. E. Shea, C. L. Scaife and K.-H. Nam, *J. Controlled Release*, 2009, **138**, 268–276.
13 P. S. Sheeran, S. Luois, P. A. Dayton and T. O. Matsunaga, *Langmuir*, 2011, **27**, 10412–10420.
14 R. Singh, G. A. Husseini and W. G. Pitt, *Ultrason. Sonochem.*, 2012, **19**, 1120–1125.
15 C. Cornelus, F. Giulieri and M.-P. K. a. G. Riess, *Colloids Surf., A*, 1993, **70**, 233–238.
16 J. Lattin, D. Belnap and W. Pitt, *Colloids Surf., B*, 2012, **89**, 93–100.
17 C. Varescon, C. Arlen, M. Le Blanc and J. G. Riess, *J. Chim. Phys.*, 1989, **86**, 2111–2117.
18 A. A. Pavia, B. Pucci, J. G. Riess and L. Zarif, *Makromol. Chem.*, 1992, **193**, 2505–2517.
19 N. Reznik, M. Seo, R. Williams, E. Bolewska-Pedyczak, M. Lee, N. Matsuura, J. Gariepy, F. S. Foster and P. N. Burns, *Phys. Med. Biol.*, 2012, **57**, 7205.
20 N. Rapoport, K.-H. Nam, R. Gupta, Z. Gao, P. Mohan, A. Payne, N. Todd, X. Liu, T. Kim, J. Shea, C. Scaife, D. L. Parker, E.-K. Jeong and A. M. Kennedy, *J. Controlled Release*, 2011, **153**, 4–5.
21 D. R. Karsa, *Fluorinated surfactants: synthesis properties applications*, ed. E. Kissa, Marcel Dekker Inc edn, 1995, vol. 36.
22 M. P. Krafft and J. G. Riess, *Biochimie*, 1998, **80**, 489–514.
23 O. Couture, P. D. Bevan, E. Chérin, K. Cheung, P. N. Burns and F. S. Foster, *Ultrasound Biol. Med.*, 2006, **32**, 73–82.
24 O. Couture, M. Faivre, N. Pannacci, A. Babataheri, V. Servois, P. Tabeling and M. Tanter, *Med. Phys.*, 2011, **38**, 1116–1123.
25 L. Zarif, J. G. Riess, B. Pucci and A. A. Pavia, *Biomater., Artif. Cells, Immobilization Biotechnol.*, 1993, **21**, 597–608.
26 L. Zarif, J. G. Riess, B. Pucci, C. Guedj and A. A. Pavia, *Artif. Cells, Blood Substitutes, Biotechnol.*, 1994, **22**, 1485–1490.
27 J. C. Maurizis, M. Azim, M. Rapp, B. Pucci, A. Pavia, J. C. Madelmont and A. Veyre, *Xenobiotica*, 1994, **24**, 535–541.
28 C. Contino-Pépin, M. C. Maurizis and B. Pucci, *Curr. Med. Chem.: Anti-Cancer Agents*, 2002, **2**, 645–665.
29 M. V. Rodnin, Y. O. Posokhov, C. Contino-Pépin, J. Brettmann, A. Kyrychenko, S. S. Palchevskyy, B. Pucci and A. S. Ladokhin, *Biophys. J.*, 2008, **94**, 4348–4357.
30 B. Pucci, J. Maurizis and A. Pavia, *Eur. Polym. J.*, 1991, **27**, 1101–1106.
31 S. Jasseron, C. Contino-Pépin, J. C. Maurizis, M. Rapp and B. Pucci, *Bioorg. Med. Chem. Lett.*, 2002, **12**, 1067–1070.
32 B. Pucci, E. Guy, F. Vial-Reveillon and A. Pavia, *Eur. Polym. J.*, 1988, **24**, 1077–1086.
33 F. Giusti, S. Mansis and B. Pucci, *New J. Chem.*, 2002, **26**, 1724–1732.
34 C. M. Starks, *Free radical telomerization*, Academic Press, 1974.
35 C. Contino, J.-C. Maurizis, M. Ollier, M. Rapp, J.-M. Lacombe and B. Pucci, *Eur. J. Med. Chem.*, 1998, **33**, 809–816.
36 D. Kozak, W. Anderson, R. Vogel and M. Trau, *Nano Today*, 2011, **6**, 531–545.
37 N. Ali, PhD thesis, Victoria University of Wellington, 2011.
38 A. V. Jagtiani, J. Zhe, J. Hu and J. Carletta, *Meas. Sci. Technol.*, 2006, **17**, 1706–1714.
39 D. W. Kupke, *Physical Principles and Techniques of Protein Chemistry*, ed. S. J. Leach, Academic Press edn, New York, 1973, vol. Part C, pp. 1–75.
40 F. Eggers and T. Funck, *Rev. Sci. Instrum.*, 1973, **44**, 969–977.
41 F. Eggers, *Acustica*, 1992, **76**, 231–240.
42 F. Eggers and U. Kaatze, *Meas. Sci. Technol.*, 1996, **7**, 1–19.
43 A. Sarvazyan, *Ultrasonics*, 1982, **20**, 151–154.
44 S. Barnartt, *J. Chem. Phys.*, 1952, **20**, 278–279.
45 B. B. Owen and H. L. Simons, *J. Phys. Chem.*, 1957, **61**, 479–482.
46 K. Sarkar and A. Prosperetti, *J. Acoust. Soc. Am.*, 1994, **96**, 332–341.
47 R. Martino, V. Gilard, F. Desmoulin and M. Malet-Martino, *J. Pharm. Biomed. Anal.*, 2005, **38**, 871–891.
48 L. Trevino, M. Postel and J. G. Riess, *J. Colloid Interface Sci.*, 1994, **166**, 414–418.
49 B. Boyer, G. Lamaty, J. Moussamou-Missima, A. Pavia, B. Pucci and J. Roque, *Eur. Polym. J.*, 1991, **27**, 1359–1363.

50 A. Kabalnov, J. Weers, R. Arlauskas and T. Tarara, *Langmuir*, 1995, **11**, 2966–2974.
51 S. S. Habif, P. E. Normand, C. B. Oleksiak and H. L. Rosano, *Biotechnol. Prog.*, 1992, **8**, 454–457.
52 C. R. Wilke and P. Chang, *AIChE J.*, 1955, **1**, 264–270.
53 J. G. Riess, *Chem. Rev.*, 2001, **101**, 2797–2920.
54 A. Kabalnov, K. Makarov and E. Shchukin, *Colloids Surf.*, 1992, **62**, 101–104.
55 A. S. Kabalnov, K. N. Makarov, O. V. Shcherbakova and A. N. Nesmeyanov, *J. Fluorine Chem.*, 1990, **50**, 271–284.
56 J. N. Marsh, C. S. Hall, S. A. Wickline and G. M. Lanza, *J. Acoust. Soc. Am.*, 2002, **112**, 2858–2862.
57 C. S. Hall, G. M. Lanza, J. H. Rose, R. J. Kaufmann, R. W. Fuhrhop, S. H. Handley, K. R. Waters, J. G. Miller and S. A. Wickline, *IEEE Trans. Ultrason. Ferroelectr. Freq. Control*, 2000, **47**, 75–84.
58 L. Cuscó and J. P. M. Trusler, *Int. J. Therm. Sci.*, 1995, **16**, 675–685.
59 D. LeGrand and G. Gaines Jr, *J. Colloid Interface Sci.*, 1975, **50**, 272–279.
60 N. Nishikido, W. Mahler and P. Mukerjee, *Langmuir*, 1989, **5**, 227–229.
61 L. Y. Clasohm, I. U. Vakarelski, R. R. Dagastine, D. Y. C. Chan, G. W. Stevens and F. Grieser, *Langmuir*, 2007, **23**, 9335–9340.
62 L. A. Halper, C. O. Timmons and W. A. Zisman, *J. Colloid Interface Sci.*, 1972, **38**, 511–516.
63 S. Sleijfer, W. H. J. Kruit and G. Stoter, *Eur. J. Cancer*, 2004, **40**, 2377–2382.
64 L. Rosiñol, M. T. Cibeira, M. Segarra, M. C. Cid, X. Filella, M. Aymerich, M. Rozman, L. Arenillas, J. Esteve, J. Bladé and E. Montserrat, *Cytokine*, 2004, **26**, 145–148.
65 C. Contino-Pépin, A. Parat, S. Périno, C. Lenoir, M. Vidal, H. Galons, S. Karlik and B. Pucci, *Bioorg. Med. Chem. Lett.*, 2009, **19**, 878–881.
66 C. Contino-Pépin, A. Parat, C. Patinote, W. A. Roscoe, S. J. Karlik and B. Pucci, *ChemMedChem*, 2010, **5**, 2057–2064.
67 L. Zarif, J. G. Riess, B. Pucci and A. A. Pavia, *Biomater., Artif. Cells, Immobilization Biotechnol.*, 1993, **21**, 597–608.
68 C. Loubat and B. Boutevin, *Polym. Bull.*, 2000, **44**, 569–576.
69 P. Barthélémy, A. Polidori and B. Pucci, in *The synthesis and biomedical applications of various telomeric structures*, ed. S. G. Pandalai, Trivandrum edn, 1999, vol. 3, pp. 117–140.
70 P. Mukerjee and K. J. Mysels, *Critical micelle concentrations of aqueous surfactant systems, Office of Standard Reference Data*, National Bureau of Standards, 1971, pp. 1–222.
71 M. J. Rosen, *Surfactants and Interfacial Phenomena*, John Wiley & Sons, Inc., 2004, pp. 105–177.
72 S. M. Bertilla, P. Marie and M.-P. Krafft, *Artificial Oxygen Carrier*, Springer Tokyo, 2005, pp. 237–251.
73 B. Abismaïl, J. Canselier, A. Wilhelm, H. Delmas and C. Gourdon, *Ultrason. Sonochem.*, 1999, **6**, 75–83.
74 S. M. Jafari, Y. He and B. Bhandari, *Eur. Food Res. Technol.*, 2007, **225**, 733–741.
75 A. Cucheval and R. Chow, *Ultrason. Sonochem.*, 2008, **15**, 916–920.
76 T. D. Martz, D. Bardin, P. S. Sheeran, A. P. Lee and P. A. Dayton, *Small*, 2012, **8**, 1876–1879.
77 T. G. Mason, J. N. Wilking, K. Meleson, C. B. Chang and S. M. Graves, *J. Phys.: Condens. Matter*, 2006, **18**, R635.
78 M. van den Tempel, *Recl. Trav. Chim. Pays-Bas*, 1953, **72**, 419–432.
79 T. Delmas, H. Piraux, A.-C. Couffin, I. Texier, F. Vinet, P. Poulin, M. E. Cates and J. Bibette, *Langmuir*, 2011, **27**, 1683–1692.
80 W. I. Higuchi and J. Misra, *J. Pharm. Sci.*, 1962, **51**, 459–466.
81 A. Kabalnov, A. Pertzov and E. Shchukin, *Colloids Surf.*, 1987, **24**, 19–32.
82 A. S. Kabalnov and E. D. Shchukin, *Adv. Colloid Interface Sci.*, 1992, **38**, 69–97.
83 Y. Enomoto, M. Tokuyama and K. Kawasaki, *Acta Metall.*, 1986, **34**, 2119–2128.
84 G. Haïat, R. Berti, B. Galaz, N. Taulier, J.-J. Amman and W. Urbach, *J. Acoust. Soc. Am.*, 2011, **129**, 1642–1652.
85 P. M. Morse and K. U. Ingard, *Theoretical Acoustics*, Princeton University Press, 1986.
86 J. J. Faran, *J. Acoust. Soc. Am.*, 2005, **23**, 405–418.
87 F. Coulouvrat, J.-L. Thomas, K. Astafyeva, N. Taulier, J.-M. Conoir and W. Urbach, *J. Acoust. Soc. Am.*, 2012, **132**, 3748–3759.
88 E. C. Unger, T. P. McCreery, R. H. Sweitzer, V. E. Caldwell and Y. Wu, *Invest. Radiol.*, 1998, **33**, 886–892.
89 M. L. Fabiilli, K. J. Haworth, I. E. Sebastian, O. D. Kripfgans, P. L. Carson and J. B. Fowlkes, *Ultrasound Biol. Med.*, 2010, **36**, 1364–1375.
90 K. Landfester, *Annu. Rev. Mater. Res.*, 2006, **36**, 231–279.
91 H. Gudbjartsson and S. Patz, *Magn. Reson. Med.*, 1995, **34**, 910–914.